Exploring Imaging Characteristics Associated With Disease Activity in Idiopathic Multifocal Choroiditis: A Multimodal Imaging Approach

EVIANNE L. DE GROOT, NINETTE H. TEN DAM-VAN LOON, CARLYN V. KOUWENBERG, JOKE H. DE BOER, AND JEANNETTE OSSEWAARDE-VAN NOREL

• PURPOSE: To identify characteristics on multimodal imaging (MMI) in idiopathic multifocal choroiditis (MFC) that can identify inflammatory activity and distinguish choroidal neovascularization (CNV) activity from inflammatory activity.

• DESIGN: Prospective cohort study.

• METHODS: MMI consisted of spectral-domain optical coherence tomography (angiography) (SD-OCT(A)), fundus autofluorescence, fundus photography, infrared imaging, fluorescein angiography (FA), and indocyanine green angiography (ICGA). MMI characteristics obtained during active and inactive disease were compared within the same lesion. Secondly, MMI characteristics were compared between active inflammatory lesions with and without CNV activity.

• RESULTS: Fifty patients (110 lesions) were included. In 96 lesions without CNV activity, the mean focal choroidal thickness was increased during the active disease (205 μm) compared to the inactive disease (180 μm) ($P \leq .001$). Lesions with inflammatory activity typically demonstrated moderately reflective material located in the sub–retinal pigment epithelium (RPE) and/or in the outer retina with disruption of the ellipsoid zone. During the inactive stage of the disease, the material disappeared or became hyperreflective and indistinguishable from the RPE. During the active stage of the disease, the area of hypoperfusion in the choriocapillaris significantly increased as visualized on both ICGA and SD-OCTA. CNV activity in 14 lesions was associated with subretinal material with a mixed reflectivity and hypotransmission of light to the choroid on SD-OCT and leakage on FA. SD-OCTA identified vascular structures in all active CNV lesions and in 24% of lesions without CNV activity (showing old, quiescent CNV membranes).

• CONCLUSION: Inflammatory activity in idiopathic MFC was associated with several MMI characteristics, including focally increased choroidal thickness. These characteristics can guide clinicians in the challenging process of the evaluation of disease activity in idiopathic MFC patients. (Am J Ophthalmol 2023;252: 45–58. © 2023 The Authors. Published by Elsevier Inc. This is an open access article under the CC BY-NC-ND license (http://creativecommons.org/licenses/by-nc-nd/4.0/))

Idiopathic multifocal choroiditis (MFC) is part of the spectrum of the "white dot syndromes" and is considered a primary inflammatory choriocapillaropathy.[1,2] Idiopathic MFC is a relapsing disease and predominantly affects Caucasian women with myopia in their second to fourth decade of life.[3,4] Typical features for idiopathic MFC are the inflammatory lesions that arise in the posterior pole at the level of the outer retina, the retinal pigment epithelium (RPE), and the choriocapillaris and the complication of secondary choroidal neovascularization (CNV). Both the inflammatory lesions and secondary CNV can be visualized and monitored using multimodal imaging (MMI) including spectral-domain optical coherence tomography (SD-OCT), spectral-domain optical coherence tomography angiography (SD-OCTA), fundus autofluorescence (FAF), and fluorescein angiography (FA) and indocyanine green angiography (ICGA).[3,5]

Monitoring and subsequently treating disease activity, even when the patient is still asymptomatic, is considered to be indicated since subclinical inflammatory disease activity can trigger the development and reactivation of secondary CNV. Moreover, subclinical inflammatory activity results in growth of the chorioretinal lesions over the years, which is, considering the young age at the first time of presentation, unfavorable.[6–8]

Currently, the evidence regarding which MMI characteristics can identify inflammatory activity is scarce and mostly limited to descriptive studies.[9–15] It can especially be challenging to recognize inflammatory activity in preexisting lesions, because the local retinal structure is already distorted. Previous studies have suggested several imaging characteristics that are associated with disease activity, including increased focal choroidal thickness on SD-OCT,[11,15] hypertransmission of the RPE on SD-OCT,[16,17] and the presence

AJO.com Supplemental Material available at AJO.com.

Accepted for publication March 18, 2023.

From the Department of Ophthalmology, University Medical Center Utrecht, Utrecht University, the Netherlands

Inquiries to Jeannette Ossewaarde-van Norel, University Medical Center Utrecht, Utrecht, the Netherlands; e-mail: a.ossewaarde-vannorel@umcutrecht.nl

0002-9394/$36.00
https://doi.org/10.1016/j.ajo.2023.03.022

of a hyperautofluorescent margin surrounding a lesion on FAF.[10,18,19]

However, most studies are cross-sectional and do not compare the same lesion over time during the active and inactive stages of disease. Therefore, it is uncertain to what extent these observed alterations during the active disease are reversible, or that they will remain altered once the inactive stage of the disease is achieved. Moreover, it is challenging to distinguish inflammatory activity from CNV activity. However, this distinction is of utmost importance, because the appropriate treatment for both conditions differs.

Therefore, the aim of this study is to identify imaging characteristics that are able to detect inflammatory activity. We will explore this by comparing the MMI results obtained during the active stage of disease with the results obtained during the inactive stage within the same patient. Moreover, we aim to find imaging characteristics distinguishing CNV activity from inflammatory activity. By identifying these imaging characteristics, we hope to provide clinicians more guidance in the challenging process to evaluate multimodal imaging in this patient group.

METHODS

This is a single-center prospective observational cohort study performed at the University Medical Center Utrecht, Utrecht, the Netherlands. The study was performed in accordance with the tenets of Helsinki, and approval for this study was waived by the institutional review board (METC Utrecht). All study participants provided written informed consent to use medical data for research purposes.

• **STUDY POPULATION:** Patients were included between April 2019 and January 2022, and the last imaging set was obtained in July 2022. All patients were diagnosed with idiopathic MFC based on predefined criteria. These criteria were in line with the later published criteria of the Standardization of Uveitis Nomenclature (SUN) criteria[20,21] with the additional criteria of posterior pole involvement and the absence of retinal vasculitis and papillitis. Alternative diagnoses were ruled out by diagnostic workup, including but not limited to tuberculosis, sarcoidosis, toxoplasmosis, and birdshot chorioretinopathy. Patients with other forms of idiopathic choroiditis including serpiginous choroiditis and relentless placoid chorioretinitis were excluded. Patients with idiopathic MFC were included in this study if 2 sets of multimodal imaging were present. The modalities ICGA, SD-OCT, and SD-OCTA had to be available in both multimodal imaging sets to be eligible for inclusion.

• **IMAGE ACQUISITION AND PROCESSING:** After pupil dilatation, all imaging modalities were performed consecutively and consisted of enhanced depth imaging SD-OCT with TruTrack Active Eye Tracking, FA-ICGA, FAF, near-infrared imaging (Spectralis HRA-OCT; Heidelberg Engineering), color fundus photography (FF 450 plus; Carl Zeiss Meditec), and SD-OCTA (SD-OCT Angioplex Cirrus HD-OCT 5000; Carl Zeiss Meditec). The imaging results of the SD-OCT existed of 1 volume of 20° × 20° (25 horizontal B-scans averaged 9 times) and 2 volumes of 20° × 5° covering the macular area (7 horizontal and 7 vertical B-scans averaged 25 times).

For acquiring FA-ICGA images, patients received standard dye dose of 4 mL of 100 mg/mL sodium fluorescein and 4 mL of 5 mg/mL indocyanine green. Information on the early and late phase was obtained and pictures were taken up until 30 minutes after injection of the dye. The Cirrus Angioplex has an A-scan rate of 68 000 per second and the AngioPlex software uses an algorithm (the "Optical Micro Angiography Complex") that is based on both amplitude and phase differences between consecutive B-scans. Both 6 × 6-mm and 3 × 3-mm SD-OCTA images from the macular area were obtained.

• **ASSESSMENT OF DISEASE ACTIVITY:** The assessment of disease activity consisted of several steps.

Step 1

An ETDRS (Early Treatment Diabetic Retinopathy Study) grid overlay was added to the ICGA image of 20 minutes for both imaging sets by one grader (E.G.). The location of the ETDRS grid was determined based on the foveal pit visualized on SD-OCT. All lesions with a diameter of more than 150 μm within the ETDRS grid on the ICGA image of both sets were numbered with a maximum of 6 lesions per eye. If more lesions could be identified, the lesions showing the most dynamism between the 2 sets were selected.

Step 2

Two experienced uveitis and/or retina specialists (J.O. and N.t.D.) assessed all lesions independently for the presence of inflammatory activity and CNV activity. Assessment was based on all available imaging results in combination with the information in the medical records regarding symptoms, ophthalmic examination, ophthalmic medical history, and treatment. Both the development of new lesions and reactivation in preexisting lesions were considered as inflammatory activity. Generally, both the development of new CNV, growth of preexistent CNV, and local exudation/hemorrhage were considered as signs of CNV activity. The lesions were scored as either active inflammation without active CNV, active inflammation with active CNV, or inactive. Disagreement was resolved by discussion.

Lesions that were scored as active in one imaging set and inactive in the other imaging set were selected for further analysis (Figure 1). In addition, for all the lesions that were scored as inflammation without active CNV, we evaluated if the lesions had signs of preexisting and inactive CNV.

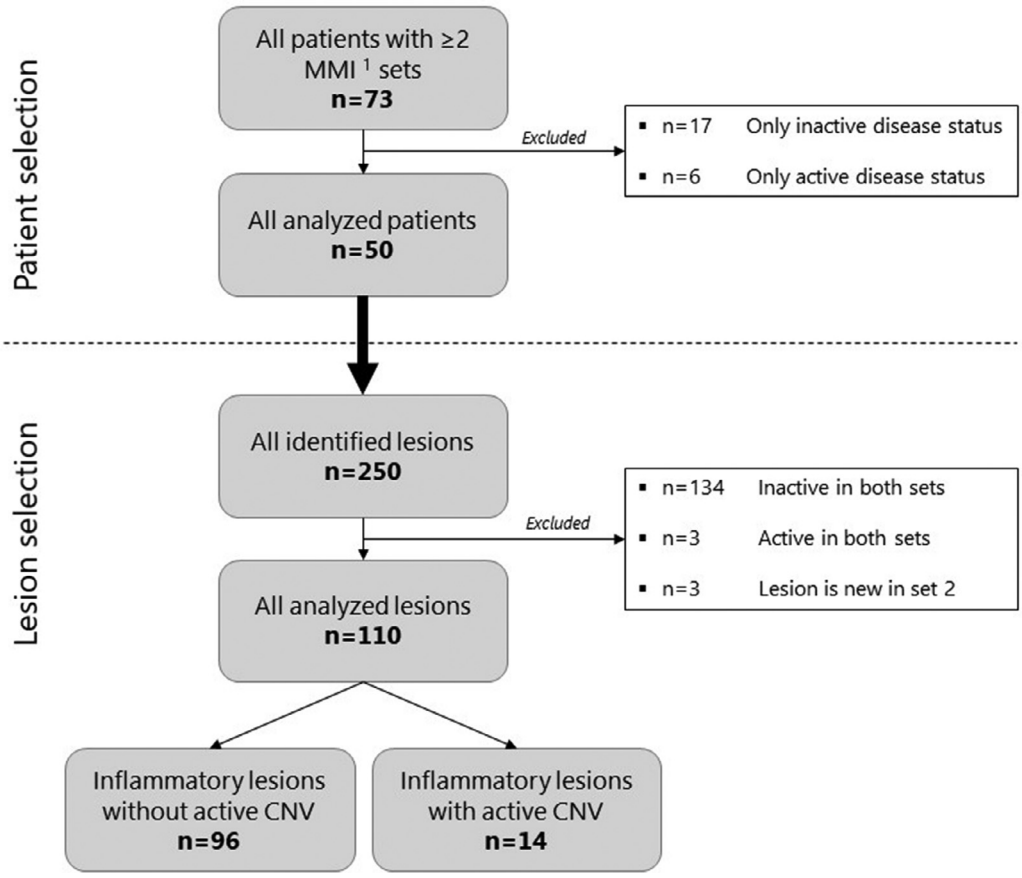

FIGURE 1. Flowchart visualizing patient and lesion selection. Patients were selected if MMI was available during the active and inactive stage of disease. In these patients, only the lesions were selected that were graded as active in one MMI set, and inactive in the other MMI set. [1]MMI included fundus photography, fundus autofluorescence, near-infrared imaging, optical coherence tomography, optical coherence tomography angiography, fluorescein angiography, indocyanine green angiography. CNV = choroidal neovascularization, MMI = multimodal imaging.

This evaluation was based on all available imaging and information from the medical records.

• **IMAGE ANALYSIS:** All imaging modalities were graded separately by the graders E.G. and C.K. (SD-OCTA by graders J.O. and E.G.). All imaging results were evaluated independently, and in case of disagreement this was resolved by discussion. Continuous variables were remeasured when values deviated by more than 20%; otherwise, results were averaged. All graders were masked for the outcome of the disease activity assessment, information from the medical records, and the results of the other imaging modalities. For a detailed description and examples of the imaging characteristics, see Supplemental Table S1 and Supplemental Figures S1-S3. The focal choroidal thickness was measured directly underneath the lesion at an identical location in both imaging sets. In addition, the choroidal thickness was measured at a single location distant from the lesions (at 3 mm extrafoveal, first or last line of the 20° × 20° horizontal SD-OCT scan) also at an identical location in both imaging sets.

SD-OCTA scans were evaluated for the presence of vascular structures and flow void, and we first assessed all slabs dynamically. To assess the presence and morphology of vascular structures on SD-OCTA in more detail, we evaluated a segmentation slab ranging from 80 µm above the RPE to 29 µm below the RPE (slab was adjusted for individual cases if needed to improve assessment). To assess the presence and extensiveness of flow void in the choriocapillaris, a segmentation slab ranging from 29 to 49 µm below the RPE was evaluated. Imaging characteristics regarding ICGA were evaluated on an image obtained in the late phase (30 ± 10 minutes). To grade fluorescence patterns on FA, early (30 seconds to 2 minutes) and late phase (10-20 minutes) images were evaluated.

• **STATISTICAL ANALYSIS:** Data analyses were performed in RStudio, version 1.2.5001 (RStudio Team), and R, version 3.6.1 (R Foundation for Statistical Computing). Imaging characteristics were compared between the active and inactive stage of the disease using the Wilcoxon signed-rank test (continuous variables) or McNemar test (categor-

ical variables). Imaging characteristics between inflammatory lesions with and without CNV activity were compared using the χ^2 test (or Fisher exact test) for categorical variables and the Wilcoxon rank-sum test for continuous variables. Correlation between variables were evaluated using the Pearson correlation coefficient. FDR of 5% was used for correcting for multiple testing. A P value of $\leq .05$ was considered significant.

RESULTS

• **STUDY PARTICIPANTS:** Multimodal imaging of 50 idiopathic MFC patients were obtained during the active and inactive stage of the disease. In total 110 chorioretinal lesions were included that were imaged during both the active and inactive stage of disease (Figure 1). Of these lesions, 96 were graded as lesions with inflammatory activity and without CNV activity and 14 lesions were graded as inflammatory activity with CNV activity. Figure 1 shows a complete overview of the process of patient and lesion selection. The patient characteristics are summarized in Table 1.

• **IMAGING CHARACTERISTICS OF LESIONS WITH INFLAMMATORY ACTIVITY:** In total, 96 lesions were analyzed that were graded as inflammatory lesions without CNV activity. Several imaging characteristics were identified that were associated with the presence of inflammatory activity (Tables 2 and 3; Figures 2-5). The most important observations on SD-OCT during inflammatory activity were (1) an increase in the focal choroidal thickness (mean 205 and 180 μm; $P < .001$); (2) the presence of moderately reflective material located sub-RPE, in the outer retina or sub-RPE with outer retina infiltration; and (3) disruption of the ellipsoid zone (EZ) ($P < .001$) and the RPE ($P < .1$).

When no inflammatory activity was present, the moderately reflective material was most likely to either disappear or become hyperreflective and indistinguishable from the RPE (Figure 2). The EZ was most likely to be absent and the RPE often remained disrupted (Figures 2 and 3). The majority of the lesions demonstrated RPE hypertransmission enhancing the signal of the choroid, independent of the presence of inflammatory activity (Table 2).

On FAF imaging, a hyperautofluorescent margin was more often observed during the presence of inflammatory activity ($P < .01$). However, note that this was only the case for 40% of the lesions and in the absence of inflammatory activity; still 20% of the lesions demonstrated a hyperautofluorescent margin (Table 3; Figure 5). The area of hypoautofluorescence on FAF was significantly lower during the presence of inflammatory activity. This most likely represents growth of the lesions over time and suggests that multimodal imaging was first obtained during the presence of inflammatory activity in the majority of the cases (Table 3; Figure 5).

All lesions were visible on ICGA imaging during the active stage of the disease, and an increase in the area of hypofluorescence on ICGA imaging was observed compared to the inactive stage of the disease (median 0.49 and 0.38 mm^2; $P < .001$). This increase was especially apparent when this area was compared to the hypoautofluorescent area on FAF. During the active stage of the disease, the SD-OCTA demonstrated flow void in 96% of the lesions, and again the area of flow void was increased (Figures 4 and 5). During the inactive stage of the disease, 96% of the lesions was visible on the ICGA image and 82% of the lesions on SD-OCTA. The hypofluorescent area on ICGA showed a high correlation with the flow void on SD-OCTA both during the presence ($r = 0.92$) and absence ($r = 0.88$) of inflammatory activity.

• **DISTINGUISHING CNV ACTIVITY FROM INFLAMMATORY ACTIVITY:** To distinguish CNV activity from inflammatory activity, we compared the lesions graded as inflammation with active CNV (n=14) with lesions graded as inflammation without active CNV (n=96). We found that signs of active CNV on SD-OCT were (1) material with a mixed reflectivity (both moderately and hyperreflective parts) in the subretinal space ($P < .001$), (2) hypotransmission of light to the choroid ($P < .05$), and (3) the presence of fluid ($P < .001$) (Figure 6). Moreover, leakage on FA was more often observed in lesions with CNV activity ($P < .01$).

SD-OCTA identified vascular structures in 100% of the lesions with CNV activity (if the imaging quality of the SD-OCTA was sufficient). Also in 20 of the inflammatory lesions without CNV activity, a vascular structure was observed. Of these 20 lesions, 19 were known to have preexistent and inactive CNV (Table 4; Figure 6). No differences in the morphology of the vascular structures were identified between the lesions with active and inactive CNV (Supplemental Table S2).

TABLE 1. Patient Characteristics

	Patients n = 50 Affected eyes n = 71
Age, y, mean (SD)	43.7 (11.8)
Female gender, n (%)	47 (94)
Bilateral disease, n (%)	21 (42)
History of CNV, n (%) of all eyes	57 (80)
Number of lesions per eye, median (IQR)	3 (2 to 5.5)
Refractive error (D), mean (SD) of all affected eyes	–5.0 (4.3)
BCVA (logMAR), median (IQR) of all affected eyes	0.027 (–0.06 to 0.20)
Time between imaging sets, d, mean (SD)	386 (224)

BCVA = best-corrected visual acuity, CNV = choroidal neovascularization, D = diopter, IQR = interquartile range.

TABLE 2. Imaging Results of Inflammatory Lesions (n=96)—SD-OCT and SD-OCTA

	Active Inflammation	Inactive Inflammation	*P* Value[a]
SD-OCT	n=96 lesions	n=96 lesions	
Location of material[b]			<.001[c]
No material	14 (15)	59 (61)	
Sub-RPE	24 (25)	6 (6)	
Indistinguishable from the RPE	10 (10)	29 (30)	
Outer retina	20 (21)	0 (0)	
Sub-RPE with outer retinal infiltration	28 (29)	2 (2)	
Reflectivity of material[b]			<.001[d]
No material	14 (15)	59 (61)	
Moderately reflective	64 (67)	6 (6)	
Hyperreflective	7 (7)	29 (30)	
Mixed	11 (11)	2 (2)	
EZ[b]			<.001[e]
Continuous	3 (3)	19 (20)	
Disrupted	85 (89)	32 (33)	
Absent	8 (8)	45 (47)	
RPE[b]			<.01[f]
Continuous	11 (11)	26 (27)	
Disrupted	83 (86)	61 (64)	
Absent	2 (2)	9 (9)	
RPE transmission[b]			.72
Normal transmission	27 (28)	26 (27)	
Hypertransmission	65 (68)	68 (71)	
Hypotransmission of light to the choroid	4 (4)	2 (2)	
Fluid			>.99
None	88 (92)	88 (92)	
Atrophic cysts (>50 μm)	7 (7)	7 (7)	
Subretinal fluid	1 (1)	1 (1)	
Intraretinal fluid (>50 μm)	0 (0)	0 (0)	
Choroidal thickness underneath the lesion in μm, mean (SD)	205 (95)	180 (95)	<.001
Choroidal thickness (distant from lesions) in μm, mean (SD)[g]	194 (70)	188 (68)	.12
SD-OCTA[h]	n=84 lesions	n=84 lesions	
Flow void visible	81 (96)	69 (82)	<.01
Blurry borders of flow void	75 (93)	60 (87)	.57
Area of flow void, mm^2, median (IQR)	0.20 (0.10-0.43)	0.16 (0.05-0.44)	<.001

EZ = ellipsoid zone, RPE = retinal pigment epithelium, SD-OCT = spectral-domain optical coherence tomography, SD-OCTA = spectral-domain optical coherence tomography angiography.

Unless otherwise noted, values are n (%).

[a]Imaging characteristics were tested with the McNemar test or the Wilcoxon signed-rank test. False discovery rate correction at 5% was applied to all the imaging characteristics in Table 2 and 3 combined.

[b]Every lesion was classified into one of the categories. If the EZ and RPE demonstrated disruption at some location in the lesion, it was graded as disrupted. The transmission of the RPE was graded according to the category that was predominantly present.

[c]The proportion of lesions with and without outer retina involvement were tested between the active and inactive disease.

[d]Both the proportion of lesions with moderately reflective material vs no material and moderately reflective material vs hyperreflective material was significantly different between the active and inactive disease.

[e]Both the proportions of lesions with absent EZ vs disrupted EZ and continuous EZ vs disrupted EZ were significantly different between the active and inactive disease.

[f]The proportion of lesions with disrupted RPE vs continuous RPE was significantly different between the active and inactive disease.

[g]The choroidal thickness was measured once per eye at 3 mm extrafoveal (first or last line of the horizontal SD-OCT scan) at a single location distant from the lesions at an identical position in both imaging sets.

[h]Missing data for 12 lesions: 11 lesions due to poor imaging quality and 1 lesion was located outside the scan area.

TABLE 3. Imaging Results of Inflammatory Lesions (n=96)—Other Imaging Modalities

	Active Inflammation	Inactive Inflammation	*P* Value[a]
Lesion visible on			
Fundus picture (n=87 [b])	84 (97)	85 (98)	>.99
Hyperpigmentation	45 (54)	48 (56)	.59
Blurry borders	67 (80)	61 (72)	.12
Hemorrhage	0 (0)	0 (0)	—
IR (n=96)	94 (98)	90 (94)	.20
Hyperreflective lesion	81 (86)	78 (87)	.59
Hyporeflective margin	53 (56)	38 (42)	.05
Blurry borders	73 (78)	57 (63)	.04
FAF (n=91[b])	86 (95)	89 (98)	.49
Hyperautofluorescent margin	34 (40)	18 (20)	<.01
Lesion area mm^2, median (IQR)	0.27 (0.10 to 0.75)	0.32 (0.13 to 0.79)	<.001
Patchy hyperautofluorescence of affected eyes (n=44)	5 (11)	2 (5)	.35
FA (n=89[b])	86 (97)	86 (97)	—
Leakage	4 (4)	0 (0)	.20
ICGA (n=96)	96 (100)	92 (96)	.20
Hypofluorescence	81 (84)	77 (84)	>.99
Blurry borders	87 (91)	72 (78)	.04
Lesion area, mm^2, median (IQR)	0.49 (0.27 to 1.25)	0.38 (0.17 to 0.92)	<.001
% difference in area FAF and ICGA, median (IQR)	74 (25 to 145)	9 (–10 to 49)	<.001

FA = fluorescein angiography, FAF = fundus autofluorescence imaging, ICGA = indocyanine green angiography, IQR = interquartile range, IR = infra-red imaging.

Unless otherwise noted, values are n (%).

[a]Imaging characteristics were tested with the McNemar test or the Wilcoxon signed-rank test. False discovery rate correction at 5% was applied to all the imaging characteristics in Table 2 and 3 combined.

[b]Missing data due to poor image quality/missing imaging: Fundus picture n = 9 lesions, FAF imaging n = 5 lesions, FA imaging n = 7 lesions.

The area of hypofluorescence on ICGA and flow void on SD-OCTA was larger in lesions with active CNV compared to all inflammatory lesions (Table 4). When comparing the lesions with active CNV (n=14) with inflammatory lesions with preexistent and inactive CNV (n=46), all imaging characteristics were still significantly different except for the area of hypofluorescence on ICGA and area of flow void on SD-OCTA. Results for all the imaging characteristics are summarized in Supplemental Tables S2 and S3.

DISCUSSION

In lesions of idiopathic MFC patients, we identified imaging characteristics associated with inflammatory activity. These characteristics included an increased focal choroidal thickness, disruption of the EZ and the presence of moderately reflective material located sub-RPE and/or in the outer retina. Moreover, we observed an increase in the hypofluorescent area on ICGA and in the area of flow void on SD-OCTA.

We showed that inflammatory activity in a lesion was associated with an increase in the focal choroidal thickness. This phenomenon was previously described by Giuffre and associates as the "sponge sign" and they observed this phenomenon in lesions with inflammatory CNV and not in myopic CNV.[15] Zhang and associates also described an increase in the choroidal thickness in lesions with inflammatory activity.[11] Interestingly, in line with the report of Zhang and associates, we also found a trend of increased choroidal thickness in the posterior pole at a distant from the focal inflammatory activity ($P = .06$; $P_{adj} = .10$). This suggests that the choroid and choriocapillaris of a large area in the posterior pole is affected by the focal inflammatory activity. In the current study, the choroidal thickness was compared within the same patient and not between patients. Therefore, our results were not influenced by the level of refractive error, age, and gender.

On ICGA, the lesions showed hypofluorescent areas that were increased in size during inflammatory activity. The hypofluorescent areas on ICGA are suggested to represent hypoperfusion of the choroid and choriocapillaris.[3,11,22,23] When inflammatory activity is absent, the hypofluorescent areas represent hypoperfusion of the lesions due to atrophy. In this case, the area corresponds with the area of RPE loss (window defect on FA and hypoautofluorescence on FAF). However, lesions with inflammatory activity demonstrate hypofluorescent areas with blurry borders extending beyond the atrophic areas. This indicates that a larger area of the choriocapillaris endures hypo- or nonperfusion.

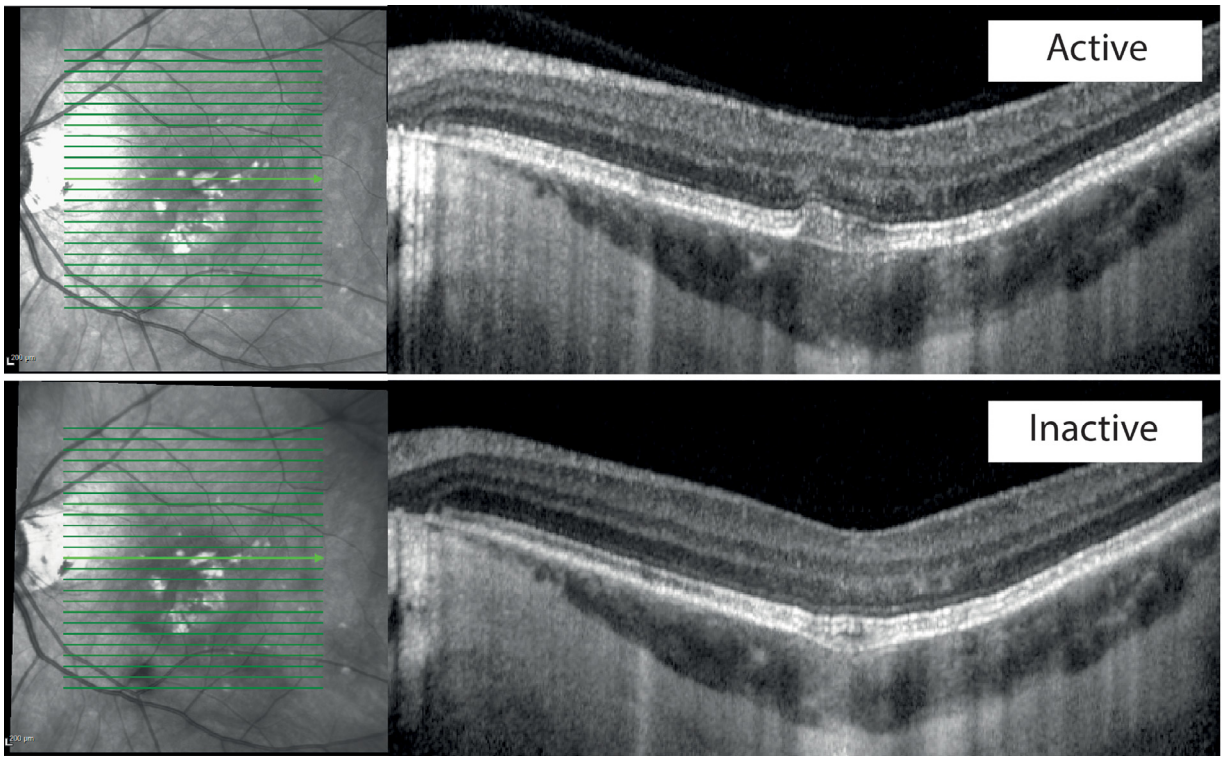

FIGURE 2. Disease activity in inflammatory lesions—Example 1. During the active stage of disease, moderately reflective sub-RPE material is observed with a disruption of the EZ and the RPE and subtle increase in the choroidal thickness below the lesion. In the inactive stage of the disease, the lesion demonstrates hyperreflective material indistinguishable from the RPE, the EZ has mostly recovered and the RPE is still disrupted. EZ = ellipsoid zone, RPE = retinal pigment epithelium.

In this study, we demonstrate that the areas of hypofluorescence on ICGA correlate with the areas of flow void on SD-OCTA and that also the area of flow void on SD-OCTA increased during inflammatory activity. Because both imaging characteristics represent choriocapillaris hypoperfusion, this finding was expected but has not been confirmed before in idiopathic MFC. In line with other reports, lesions with inflammatory activity typically demonstrated moderately reflective sub-RPE material often infiltrating the outer retina with disruption of the EZ and RPE.[10,11,13,24] When inflammatory activity was not present, this material was most likely to disappear or become hyperreflective, the RPE often remains disrupted, and the EZ was most likely to disappear.

We suggest that this shift from moderately reflective to hyperreflective material or vice versa is the result of the development of fibrosis (hyperreflective) in the inactive stage, which can again become moderately reflective after the infiltration of inflammatory cells. The EZ and RPE are most likely disrupted because of infiltration of inflammatory cells and local ischemia due to the hypoperfusion of the choriocapillaris.

In this study, no variables related to fundus photography were associated with inflammatory activity. Historically, fundus photography visualizes inflammatory activity in lesions as blurry and creamish-white-colored regions in the posterior pole.[4,11] Perhaps this is only the case for new lesions, and most lesions assessed in this study were preexisting with reactivation of the inflammatory activity. We suggest that fundus photography is able to identify inflammatory activity in new lesions, but has a low sensitivity for the detection of inflammatory activity in preexisting lesions.

Additionally, we found that CNV activity was associated with the presence of a vascular structure on SD-OCTA, leakage on FA, and mixed reflective subretinal material and hypotransmission of light to the choroid on SD-OCT. Loss of signal in the choroid has previously been associated with secondary CNV and is most likely the result of blockage of the SD-OCT signal by the vascular structure.[12,16,25] In the current study, hypotransmission was more often present in lesions with CNV activity compared to lesions with inflammatory activity. However, the majority of the lesions with CNV activity demonstrated predominantly RPE hypertransmission.

The hypotransmission of light to the choroid is often transient and is only associated with active CNV and becomes less frequent when the CNV is inactive. Moreover, lesions with CNV activity often demonstrated mixed reflectivity within the lesion, which could be used to distinguish CNV from inflammation. Nevertheless, note that this is

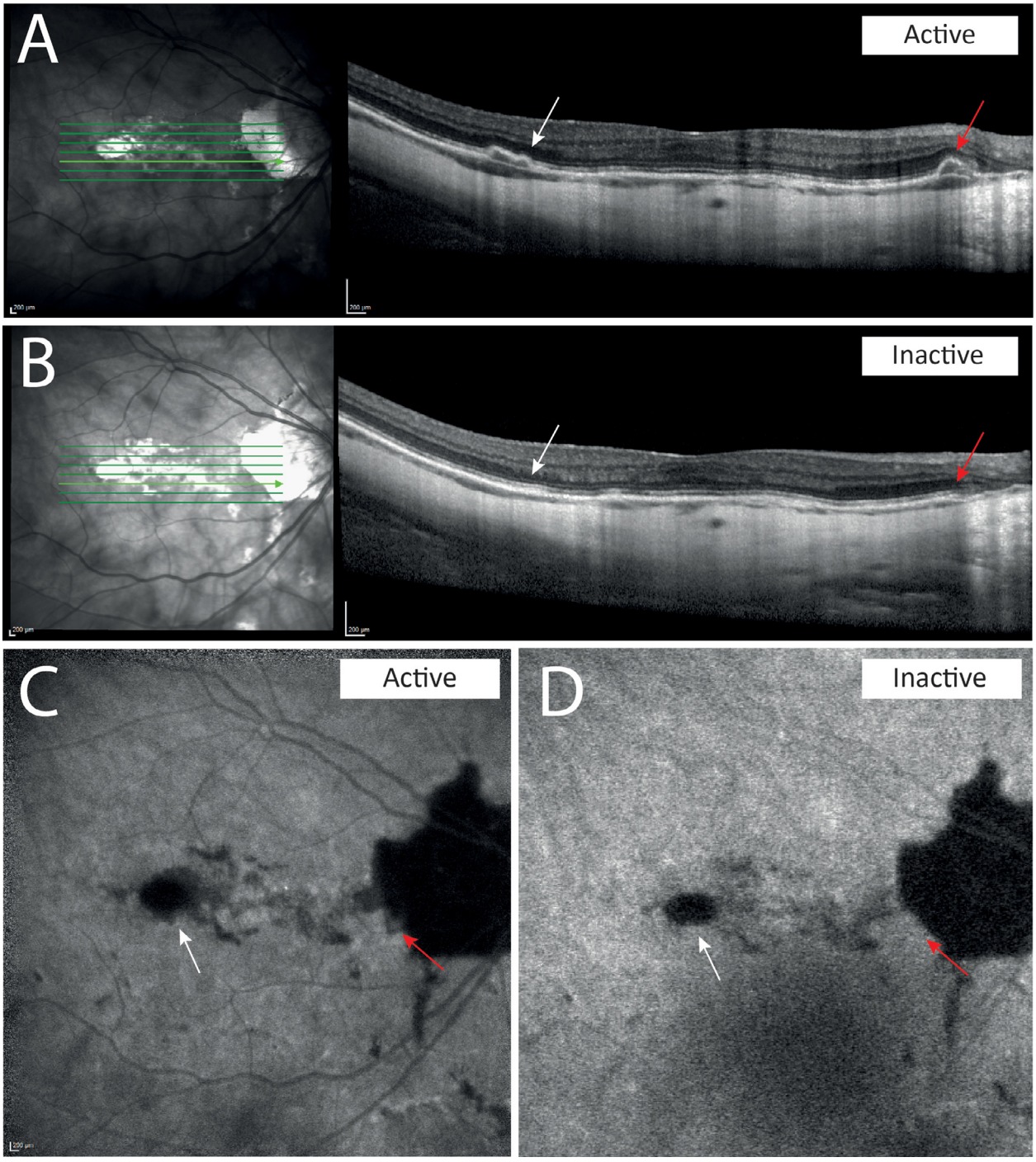

FIGURE 3. Disease activity in inflammatory lesions—Example 2. A. Two active lesions can be identified on this SD-OCT image indicated with the white and red arrow. Disease activity can be recognized by the increased choroidal thickness beneath the lesions, moderately reflective material located either sub-RPE (white arrow) or sub-RPE with outer retinal infiltration (red arrow). B. During the inactive stage, normalization of the choroidal thickness can be observed with disappearance of the moderately reflective material. C. The ICGA image taken after 20 minutes during active disease shows blurry hypofluorescent areas at the location of both lesions. D. The ICGA image taken after 20 minutes during inactive disease shows disappearance of the blurry hypofluorescent areas (red arrow) or decrease in size of the areas (white arrow). ICGA = indocyanine green angiography, RPE = retinal pigment epithelium, SD-OCT = spectral-domain optical coherence tomography.

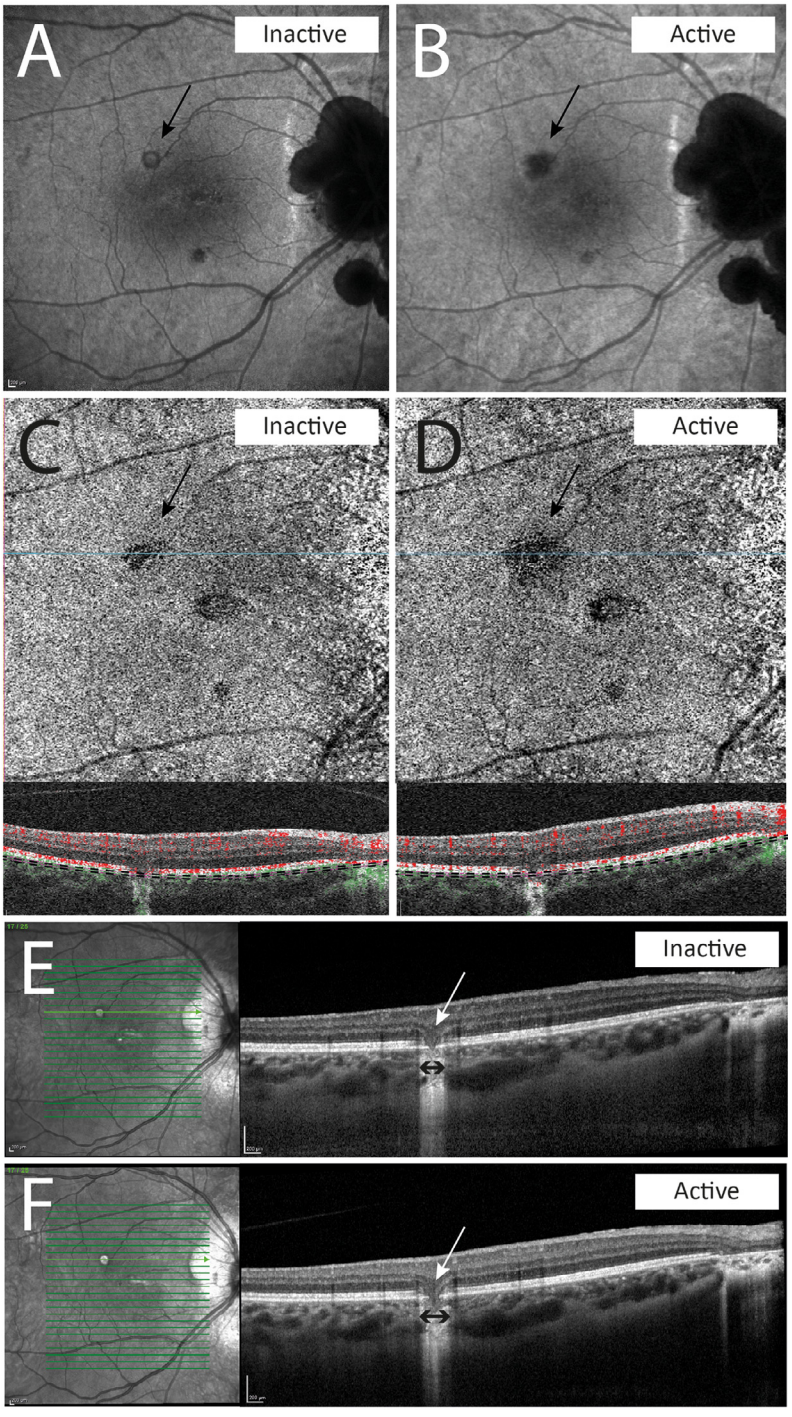

FIGURE 4. Disease activity in inflammatory lesion—Example 3. During the inactive stage of disease, we observe a hypofluorescent area with sharp boundaries on the ICGA image (A), a small area of flow void in the choriocapillaris slab (black dotted lines represents the upper and lower boundaries of this slab) on the SD-OCTA image (C), absent EZ and absent RPE in a small area on the SD-OCT (E). During the active stage of the disease, we observe an increased hypofluorescent area with blurry boundaries on the ICGA image (B), corresponding with an increased area of flow void in the choriocapillaris on SD-OCTA (D). On the SD-OCT (F), no clear signs of disease activity can be identified. The choroidal thickness is not increased, there is no material visible, and the EZ and RPE are still absent. The width of the area of EZ and RPE absence and hypertransmission of the RPE has slightly increased as indicated with the double black arrows. EZ = ellipsoid zone, ICGA = indocyanine green angiography, RPE = retinal pigment epithelium, SD-OCTA = spectral-domain optical coherence tomography angiography, SD-OCT = spectral-domain optical coherence tomography.

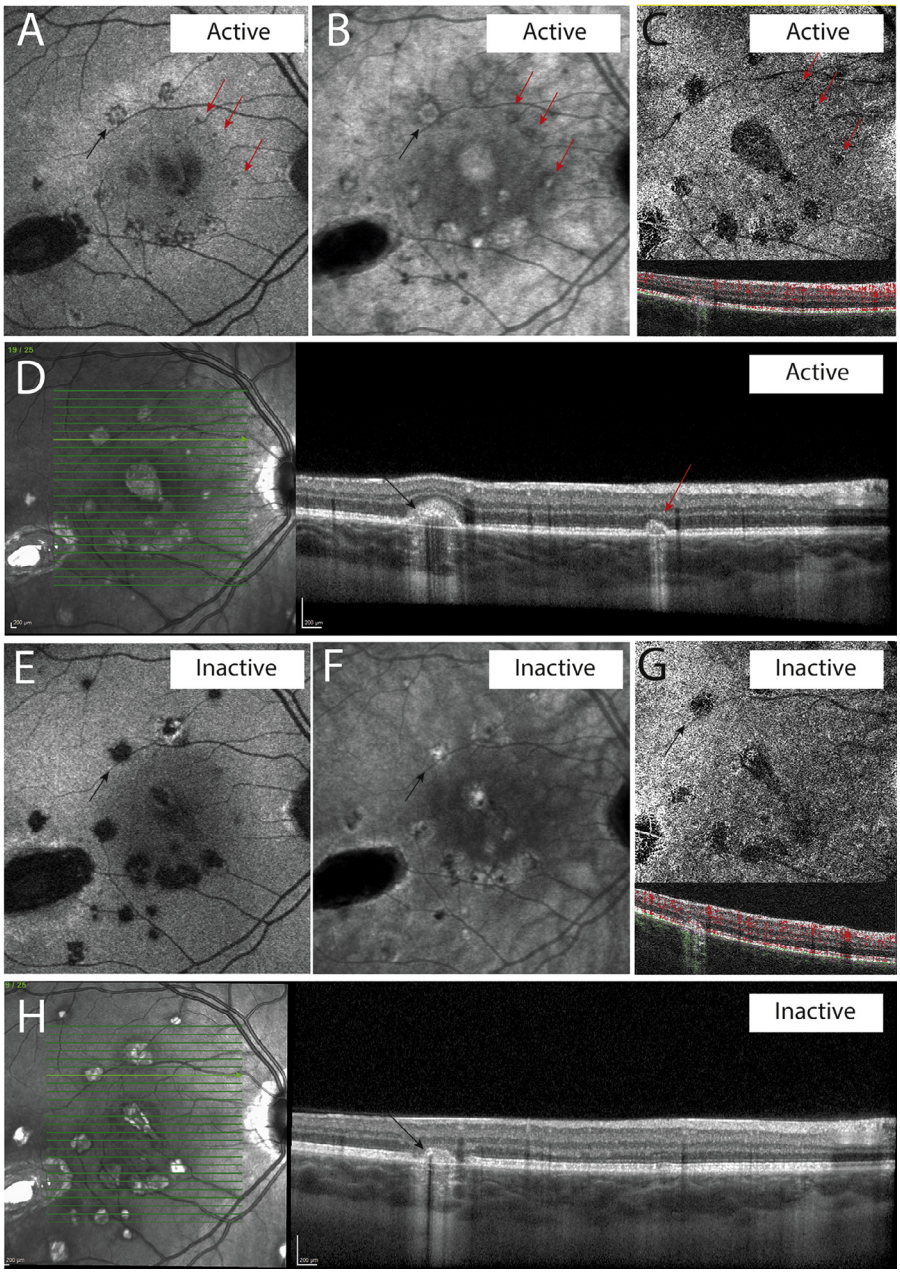

FIGURE 5. Inflammatory and CNV activity in multiple lesions—Example 4. Black arrow indicates an inflammatory lesion with an active CNV, the red arrows indicate inflammatory lesions without CNV. A and E. FAF imaging demonstrating considerable growth of the hypoautofluorescent areas between the 2 sets. Hyperautofluorescent halo (black arrow) can be observed surrounding several lesions during active disease (A), which is absent for the majority of the lesions during the inactive disease (E). B and F. ICGA imaging taken at 30 minutes after injection of dye. Large and blurry areas of hypofluorescence during active disease (B) mostly decreasing in size (black arrow) or resolving (red arrows) during inactive disease (F). C and G. SD-OCTA images of the choriocapillaris slab demonstrating large areas of hypoperfusion during active disease (C). During the inactive disease (G), some of these areas decrease (black arrow) or completely resolve (red arrows) and some have increased because of growth of the atrophic areas. D and H. SD-OCT images. During the active disease (D) the lesion indicated with the black arrow demonstrates both subretinal and sub-RPE material with EZ and RPE disruption in the active phase with mixed reflectivity of the material. For the lesion indicated with the red arrow, during the active stage sub-RPE moderately reflective material arises with RPE hypertransmission. In the inactive phase (H), in the lesion with the black arrow the subretinal material disappears, the EZ is absent, and the RPE remains disrupted. For the lesion with red arrow, the lesion has completely resolved with restoration of the RPE and EZ layers and the disappearance of the RPE hypertransmission. CNV = choroidal neovascularization, EZ = ellipsoid zone, FAF = fundus autofluorescence, ICGA = indocyanine green angiography, RPE = retinal pigment epithelium, SD-OCTA = spectral-domain optical coherence tomography angiography, SD-OCT = spectral-domain optical coherence tomography.

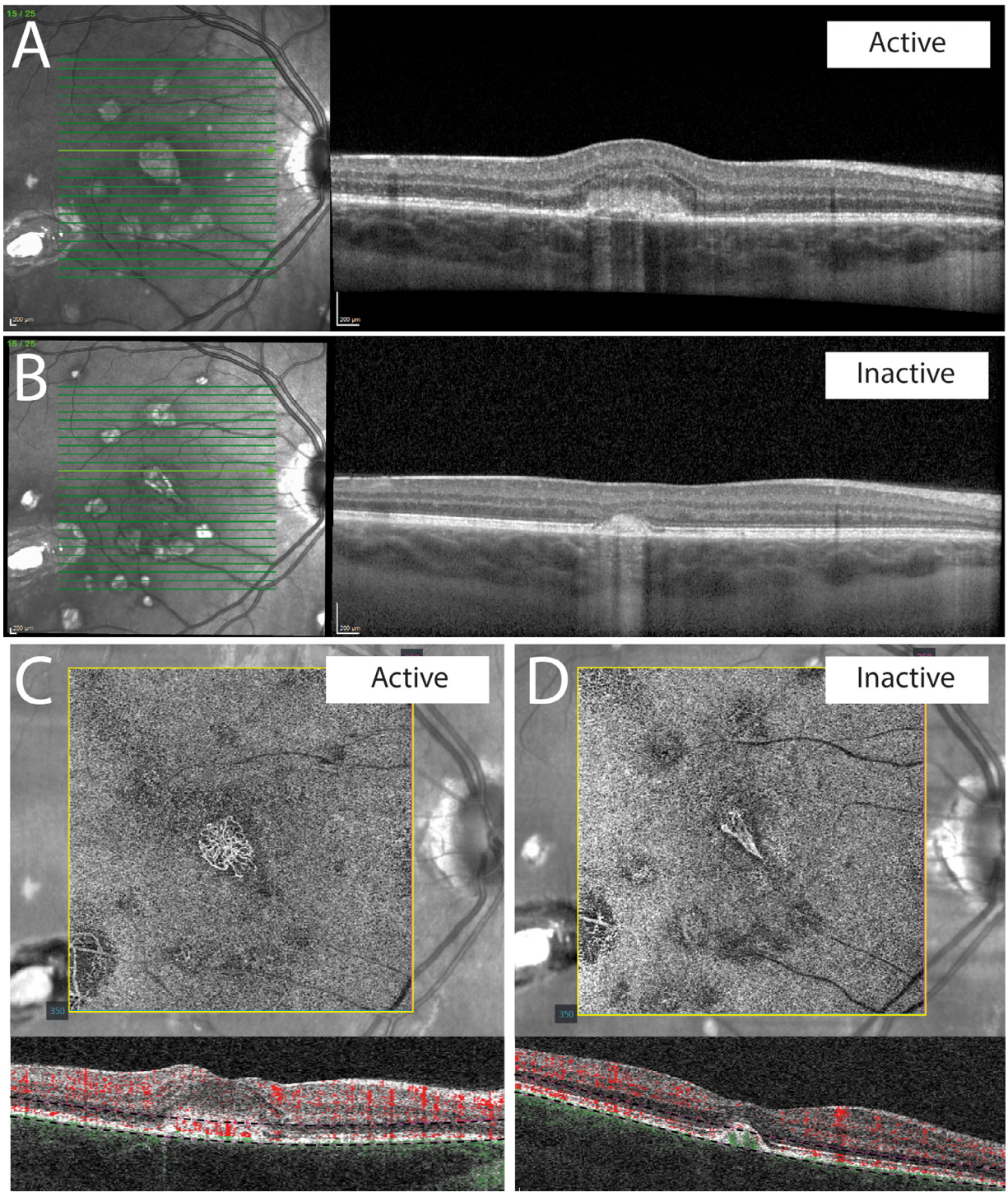

FIGURE 6. CNV activity. A and B. SD-OCT images. During the active phase (A), both moderately reflective and hyperreflective material in the subretinal space and sub-RPE can be observed with disruption of both the RPE and EZ with predominantly hypotransmission of light to the choroid. During the inactive phase (B), the subretinal moderately reflective material disappears and the RPE shows predominantly hypertransmission. C and D. SD-OCTA images of a slab between 80 μm above the RPE till 29 μm below the RPE (black dotted lines represents the upper and lower boundaries of this slab). A vascular structure is visible both during the active and inactive disease. During the active disease, both the area of the vascular network as the area of hypoperfusion or "halo" surrounding the vascular network are larger. CNV = choroidal neovascularization, EZ = ellipsoid zone, FA = fluorescein angiography, RPE = retinal pigment epithelium, SD-OCT = spectral-domain optical coherence tomography, SD-OCTA = spectral-domain optical coherence tomography angiography.

TABLE 4. Imaging Characteristics Related to Activity of Choroidal Neovascularization

	Inflammation With Active CNV (n=14 Lesions)	Inflammation Without Active CNV (n=96 Lesions)	*P* Value[a]
Location of material on SD-OCT			<.001
No material	0 (0)	14 (15)	
Sub-RPE	1 (7)	24 (25)	
Indistinguishable from the RPE	2 (14)	10 (10)	
Subretinal*	5 (36)	0 (0)	
Outer retina	0 (0)	20 (21)	
Sub-RPE with outer retinal infiltration	0 (0)	28 (29)	
Sub-RPE and subretinal*	6 (43)	0 (0)	
Reflectivity of the material on SD-OCT			<.001
No material	0 (0)	14 (15)	
Moderately reflective*	1 (7)	64 (67)	
Hyperreflective	0 (0)	7 (7)	
Mixed*	13 (93)	11 (11)	
RPE transmission on SD-OCT			<.05
Normal transmission	3 (21)	27 (28)	
Hypertransmission	6 (43)	65 (68)	
Hypotransmission of light to the choroid*	5 (36)	4 (4)	
Fluid on SD-OCT			<.001[b]
No fluid	7 (50)	88 (92)	
Intraretinal fluid	5 (36)	0 (0)	
Subretinal fluid (>50 μm)	5 (36)	1 (1)	
Atrophic cysts (>50 μm)	2 (14)	7 (7)	
Leakage on FA[c]	6 (46)	4 (4)	<.01
Hypofluorescent area on ICGA, median (IQR)	1.72 (1.21-1.87)	0.49 (0.27-1.25)	<.01[d]
Vascular structure on SD-OCTA	12[e] (100)	20[e] (24)	<.001
Area of flow void on SD-OCTA, median (IQR)	0.54 (0.43-1.27)	0.22 (0.11-0.51)	<.01[d]

CNV = choroidal neovascularization, FA = fluorescein angiography, ICGA = indocyanine green angiography, RPE = retinal pigment epithelium, SD-OCT = spectral-domain optical coherence tomography, SD-OCTA = spectral-domain optical coherence tomography angiography.

Unless otherwise noted, values are n (%).

[a]Results of the χ^2 test (or Fisher exact test) for categorical variables and the Wilcoxon rank-sum test for continuous variables. False discovery rate at 5% was applied for all tested imaging characteristics to correct for multiple testing. The categories that demonstrated significantly different proportions between inflammatory lesions with and without active CNV are indicated with an asterisk (*).

[b]The presence of fluid vs no fluid was tested (atrophic cysts were not included in the analysis).

[c]In one case with active CNV, no FA was performed because of a fluorescein allergy.

[d]When comparing the 14 lesions with active CNV with the 46 lesions with preexistent and inactive CNV, these imaging characteristics were no longer significant.

[e]SD-OCTA was not available for some lesions because of poor image quality or severe artifacts (2 lesions with active CNV and 12 lesions without active CNV).

not pathognomonic because inflammatory lesions also can demonstrate mixed reflectivity in the lesion.

Interestingly, Chen and associates reported that RPE disruption and RPE hypertransmission are early signs of secondary CNV.[17] We suggest that these imaging characteristics implicate inflammatory activity, which subsequently is able to trigger the development of secondary CNV, explaining the association with secondary CNV. In line with other reports, we confirm that lesions with CNV activity demonstrated vascular structures on SD-OCTA imaging.[12,26–29] However, we suggest that OCTA imaging is particularly useful to detect CNV activity in new lesions or lesions without a history of CNV activity. We also demonstrate in this study that the SD-OCTA seems less useful for detecting CNV activity in lesions with a history of CNV, because these lesions often still demonstrate flow on the SD-OCTA.[26,28]

It is still subject of debate what the initially targeted structure is in idiopathic MFC. Some advocate the outer segments of the photoreceptors are first targeted in idiopathic MFC and that subsequently the recruitment of inflammatory cells results in hypoperfusion of the choriocapillaris, increase in the choroidal thickness, and the accumulation of material in the outer retina and under the RPE.[11] Others believe that the choriocapillaris is first targeted, resulting in hypoperfusion in the choriocapillaris with subsequent ischemia. In line with this theory, the local ischemia will result in the alterations observed in the EZ layer and recruitment of inflammatory cells.[30]

Interestingly, in Figure 4 we show a case with inflammatory activity in a lesion that only demonstrated increased hypoperfusion in the choriocapillaris without other signs of inflammatory activity, including no increase in the choroidal thickness and no accumulation of material under the RPE or in the outer retina. Even though no direct conclusions can be drawn, this suggests that the initially targeted structure is indeed the choriocapillaris.

We believe our results can be used in future studies to improve the monitoring of patients with idiopathic MFC. Future studies could explore the positive and negative predictive value of these imaging characteristics using a larger cohort and a cross-sectional study design. In this study, we measured the choroidal thickness only at a single location for each lesion. In case of choroidal excavation, an additional line was drawn to simulate the normal retinal structure to avoid overestimation of the difference of the choroidal thickness between the active and the inactive stage. Note that the number of cases with choroidal excavation was low and therefore the influence on the outcomes in this study was limited.

Future studies regarding automated quantification of choroidal parameters, including choroidal thickness and total choroidal volume, could investigate whether these variables can be used for the early detection of disease activity.[31] Moreover, it would be interesting to explore the choroidal thickness and visualization of flow voids using the additional swept-source technology. Furthermore, in this study not all lesions could be assessed on SD-OCTA imaging because of poor imaging quality and severe artifacts, especially in patients with very high myopia.

The technology regarding OCTA imaging is continuously evolving, and we believe this imaging modality will have a prominent position in the monitoring of idiopathic MFC patients in the future. In the current study, we measured the area of flow voids manually, making this a time-consuming measurement not suitable for clinical practice. If this could be automatized using specific algorithms, this would probably improve the accuracy of this measurement and make it suitable for clinical practice. Ideally, the OCTA would eventually replace the invasive imaging modality ICGA for visualization of hypoperfusion in the choriocapillaris. The areas of hypoperfusion are shown to respond to therapy in small case studies[32,33] and could perhaps be used in the future as end points for larger clinical trials concerning the treatment of idiopathic MFC.

Strengths of the current study were the relatively high number of included patients and the evaluation of the same lesions between the active and inactive stage of the disease. A limitation of this study is the absence of absolute criteria to determine activity in a lesion. To minimize the effect of this limitation, we deliberately included 2 clinical experts and 2 nonclinical graders, who all independently scored the imaging characteristics. The experts considered all the features together, whereas the nonclinical graders considered each imaging feature separately, without knowing the disease activity status. Although we recognize the lack of a gold standard, we carefully weighted all options and trust that the independent judgement of 2 experienced clinicians is an appropriate alternative.

Other limitations of this study were the low number of lesions with CNV activity, resulting in limited power to detect imaging characteristics indicating CNV activity. Moreover, the image quality of the SD-OCTA was too poor for evaluation in a considerable proportion of the lesions. Lastly, both because of technical reasons and the COVID-19 pandemic, not all imaging modalities were available in all cases.

In conclusion, inflammatory activity in idiopathic MFC patients is associated with an increased focal choroidal thickness, moderately reflective material in the outer retina with disruption of the EZ, and increased areas of hypoperfusion in the choriocapillaris. These imaging characteristics can guide clinicians in the challenging process to evaluate disease activity on multimodal imaging in idiopathic MFC patients.

THE AUTHORS INDICATE NO FINANCIAL SUPPORT OR CONFLICTS OF INTEREST. ALL AUTHORS ATTEST THAT THEY MEET THE CURRENT ICMJE CRITERIA FOR AUTHORSHIP.
Funding/Support: This work was supported by the Dr. F.P. Fischer Foundation, Foundation Beheer het Schild, Landelijke Stichting voor Blinden en Slechtzienden (LSBS), Rotterdamse Stichting Blindenbelangen (RBS), Foundation Louise Rottinghuis, and Oogfonds.

REFERENCES

1. Papasavvas I, Herbort CPJ. Diagnosis and treatment of primary inflammatory choriocapillaropathies (PICCPs): a comprehensive overview. *Medicina (B Aires)*. 2022;58(2):165. doi:10.3390/medicina58020165.
2. Neri P, Herbort CP, Hedayatfar A, et al. White dot syndromes", an inappropriate and outdated misnomer. *Int Ophthalmol*. 2022;42(1):1–6. doi:10.1007/s10792-021-02121-4.
3. Ahnood D, Madhusudhan S, Tsaloumas MD, Waheed NK, Keane PA, Denniston AK. Punctate inner choroidopathy: a review. *Surv Ophthalmol*. 2017;62(2):113–126. doi:10.1016/j.survophthal.2016.10.003.
4. Tavallali A, Yannuzzi LA. Idiopathic multifocal choroiditis. *J Ophthalmic Vis Res*. 2016;11(4):429–432. doi:10.4103/2008-322X.194141.
5. Fung AT, Pal S, Yannuzzi NA, et al. Multifocal choroiditis without panuveitis; clinical characteristics and progression. *Retina*. 2014;34(1):98–107. doi:10.1097/IAE.0b013e31829234cb.
6. Chen YC, Chen YL, Chen SN. Chorioretinal atrophy in punctate inner choroidopathy/multifocal choroiditis: a five-

year follow-up study. *Ocul Immunol Inflamm*. 2022;30(2):270–275. doi:10.1080/09273948.2020.1869269.
7. Erba S, Cozzi M, Xhepa A, Cereda M, Staurenghi G, Invernizzi A. Distribution and progression of inflammatory chorioretinal lesions related to multifocal choroiditis and their correlations with clinical outcomes at 24 months. *Ocul Immunol Inflamm*. 2022;30(2):409–416. doi:10.1080/09273948.2020.1800048.
8. de Groot EL, de Boer J, Ossewaarde-van Norel J. Idiopathic multifocal choroiditis and punctate inner choroidopathy: evaluation of risk factors for increased relapse rate. A 2-year prospective observational cohort study. *Ophthalmologica*. 2022 Published online. doi:10.1159/000526663.
9. Pohlmann D, Pleyer U, Joussen AM, Winterhalter S. Optical coherence tomography angiography in comparison with other multimodal imaging techniques in punctate inner choroidopathy. *Br J Ophthalmol*. 2019;103:60–66.
10. Li J, Li Y, Li H, Zhang L. Imageology features of different types of multifocal choroiditis. *BMC Ophthalmol*. 2019;19(1):1–7. doi:10.1186/s12886-019-1045-x.
11. Zhang X, Zuo C, Li M, Chen H, Huang S, Wen F. Spectral-domain optical coherence tomographic findings at each stage of punctate inner choroidopathy. *Ophthalmology*. 2013;120(12):2678–2683. doi:10.1016/j.ophtha.2013.05.012.
12. Cheng L, Chen X, Weng S, et al. Spectral-domain optical coherence tomography angiography findings in multifocal choroiditis with active lesions. *Am J Ophthalmol*. 2016;169:145–161. doi:10.1016/j.ajo.2016.06.029.
13. Channa R, Ibrahim M, Sepah Y, et al. Characterization of macular lesions in punctate inner choroidopathy with spectral domain optical coherence tomography. *J Ophthalmic Inflamm Infect*. 2012;2(3):113–120. doi:10.1007/s12348-011-0054-6.
14. Zarranz-Ventura J, Sim DA, Keane PA, et al. Characterization of punctate inner choroidopathy using enhanced depth imaging optical coherence tomography. *Ophthalmology*. 2014;121(9):1790–1797. doi:10.1016/j.ophtha.2014.03.011.
15. Giuffrè C, Marchese A, Fogliato G, et al. The "sponge sign": a novel feature of inflammatory choroidal neovascularization. *Eur J Ophthalmol*. 2021;31(3):1240–1247. doi:10.1177/1120672120917621.
16. Shi X, Cai Y, Luo X, Liang S, Rosenfeld PJ, Li X. Presence or absence of choroidal hyper-transmission by SD-OCT imaging distinguishes inflammatory from neovascular lesions in myopic eyes. *Graefes Arch Clin Exp Ophthalmol*. 2020;258(4):751–758. doi:10.1007/s00417-019-04571-0.
17. Chen Y, Chen Q, Li X, Li M. RPE disruption and hypertransmission are early signs of secondary CNV with punctate inner choroidopathy in structure-OCT. *BMC Ophthalmol*. 2021;21(1):427. doi:10.1186/s12886-021-02197-7.
18. Turkcuoglu P, Chang PY, Rentiya ZS, et al. Mycophenolate mofetil and fundus autofluorescence in the management of recurrent punctate inner choroidopathy. *Ocul Immunol Inflamm*. 2011;19(4):286–292. doi:10.3109/09273948.2011.580072.
19. Li M, Zhang X, Wen F. The fundus autofluorescence spectrum of punctate inner choroidopathy. *J Ophthalmol*. 2015;2015:202097. doi:10.1155/2015/202097.
20. The Standardization of Uveitis Nomenclature (SUN) Working group. Classification criteria for punctate inner choroiditis. *Am J Ophthalmol*. 2021;228:275–280. doi:10.1016/j.ajo.2021.03.046.
21. The Standardization of Uveitis Nomenclature (SUN) Working group. Classification criteria for multifocal choroiditis with panuveitis. *Am J Ophthalmol*. 2021;228:152–158. doi:10.1016/j.ajo.2021.03.043.
22. Herbort CP. Fluorescein and indocyanine green angiography for uveitis. *Middle East Afr J Ophthalmol*. 2009;16(4):168–187. doi:10.4103/0974-9233.58419.
23. Dingerkus VLS, Munk MR, Brinkmann MP, et al. Optical coherence tomography angiography (OCTA) as a new diagnostic tool in uveitis. *J Ophthalmic Inflamm Infect*. 2019;9(1):10. doi:10.1186/s12348-019-0176-9.
24. Amer R, Priel E, Kramer M. Spectral-domain optical coherence tomographic features of choroidal neovascular membranes in multifocal choroiditis and punctate inner choroidopathy. *Graefes Arch Clin Exp Ophthalmol*. 2015;253(6):949–957. doi:10.1007/s00417-015-2930-5.
25. Agarwal A, Handa S, Marchese A, et al. Optical coherence tomography findings of underlying choroidal neovascularization in punctate inner choroidopathy. *Front Med (Lausanne)*. 2021;8:758370. doi:10.3389/fmed.2021.758370.
26. Astroz P, Miere A, Mrejen S, et al. Optical coherence tomography angiography to distinguish choroidal neovascularization from macular inflammatory lesions in multifocal choroiditis. *Retina*. 2018;38:299–309.
27. Levison AL, Baynes KM, Lowder CY, Kaiser PK, Srivastava SK. Choroidal neovascularisation on optical coherence tomography angiography in punctate inner choroidopathy and multifocal choroiditis. *Br J Ophthalmol*. 2017;101:616–622.
28. Dutheil C, Korobelnik JF, Delyfer MN, Rougier MB. Optical coherence tomography angiography and choroidal neovascularization in multifocal choroiditis: a descriptive study. *Eur J Ophthalmol*. 2018;28(5):614–621. doi:10.1177/1120672118759623.
29. Zahid S, Chen KC, Jung JJ, et al. Optical coherence tomography angiography of chorioretinal lesions due to idiopathic multifocal choroiditis. *Retina*. 2017;37(8):1451–1463. doi:10.1097/IAE.0000000000001381.
30. Herbort CP, Tugal-Tutkun I, Mantovani A, Neri P, Khairallah M, Papasavvas I. Advances and potential new developments in imaging techniques for posterior uveitis, Part 2: invasive imaging methods. *Eye*. 2021;35(1):52–73. doi:10.1038/s41433-020-1072-0.
31. Khaing TT, Okamoto T, Ye C, et al. Automatic measurement of choroidal thickness and vasculature in optical coherence tomography images of eyes with retinitis pigmentosa. *Artif Life Robot*. 2022;27(1):70–79. doi:10.1007/s10015-022-00737-y.
32. Agarwal A, Abhaypal K, Aggarwal K, et al. The use of optical coherence tomography angiography in comparing choriocapillaris recovery between two treatment strategies for multifocal choroiditis: a pilot clinical trial. *J Ophthalmic Inflamm Infect*. 2022;12(1):12. doi:10.1186/s12348-022-00291-5.
33. Thompson IA, Caplash S, Akanda M, et al. Optical coherence tomography angiography changes in choroidal vasculature following treatment in punctate inner choroidopathy. *Ocul Immunol Inflamm*. 2021;29(5):944–950. doi:10.1080/09273948.2019.1705986.